Journal of Solid State Chemistry **143,** 254–259 (1999)
Article ID jssc.1998.8102, available online at http://www.idealibrary.com on IDEAL®

Rodalquilarite Revisited: The Hydrothermal Synthesis and Structural Reinvestigation of $H_3Fe_2(TeO_3)_4Cl$

Christopher R. Feger,* Joseph W. Kolis,* Krzysztof Gorny,† Charles Pennington†

*Department of Chemistry, Clemson University, Clemson, South Carolina 29634; and †Department of Physics, The Ohio State University, Columbus, Ohio 43210

Received March 9, 1998; in revised form November 10, 1998; accepted November 22, 1998

The known mineral rodalquilarite, $H_3Fe_2(TeO_3)_4Cl$, was obtained as high quality single crystals via hydrothermal reactions. This material crystallizes in the triclinic space group, $P\bar{1}$, with cell constants of $a = 5.103(2)$ Å, $b = 6.653(2)$ Å, $c = 9.012(3)$ Å, $\alpha = 73.40(2)^\circ$, $\beta = 78.03(2)$, $\gamma = 76.76(2)$, $V = 282.1(2)$ Å^3 and was obtained from an NH_4Cl solution that was heated at 375°C for 4 days. A detailed structural characterization was performed ($R = 0.039$, $R_w = 0.050$) and showed that this material is based on layers consisting of edge-sharing FeO_6 octahedra which are interconnected by TeO_3 pyramids which are completed by the presence of a terminal hydrogen atom. Additionally, a second set of TeO_3 pyramids attached to the FeO_6 octahedra are linked across the layers by a shared hydrogen atom. The layers are held together only through these O–H–O interactions and additional weak Te–Cl interactions.

In this study, we compare this structure to a previous report of rodalquilarite and a reported triclinic form of $Fe_2Te_4O_{11}$, which may have been misidentified and is also the title compound. In addition, we have obtained the band gap of this material by diffuse reflectance spectroscopy and find it to be a wide band gap ($E_g = 2.51$ eV) material. The DC magnetic susceptibility was also obtained and showed that the title compound is antiferromagnetic with a T_N of 29 K.

INTRODUCTION

In our studies of first row transition metal tellurites, we identified the $M_2Te_3O_8$ system as an interesting series of compounds that are isostructural to the mineral spiroffite (1). We were able to identify a continuous series of these compounds containing divalent metals from manganese to zinc, with the lone exception being iron. During these investigations, we find that iron compounds run under hydrothermal conditions typically contain trivalent iron. To that end, using an ammonium chloride mineralizer, we have obtained high quality single crystals of the previously characterized but unusual mineral rodalquilarite, $H_3Fe_2(TeO_3)_4Cl$ (2).

In our review of the literature, we have found several iron tellurites, including a pair of compounds with the reported formula of $Fe_2Te_4O_{11}$ (3, 4). In our review of the report of triclinic $Fe_2Te_4O_{11}$ (4), we believe that this material was actually rodalquilarite, as based on its X-ray powder diffraction pattern and lattice constants. In this paper, we report an excellent synthesis for rodalquilarite and a detailed reinvestigation of the single crystal structure which yielded a determination of the hydrogen positions, as well as magnetic and diffuse reflectance data.

EXPERIMENTAL

Synthesis

Reaction conditions used to obtain $H_3Fe_2(TeO_3)_4Cl$ were very similar to those used to obtain the $M_2Te_3O_8$ phases. $FeCl_2 \cdot 4H_2O$ (89 mg, Fisher, 99.9%) and TeO_2 (143 mg, Strem, 99 + %) were sealed in fused silica tubing with 1 *M* NH_4Cl solution, placed in an autoclave which was pressurized with argon to ~2500 psi, and subsequently heated to 375°C for 4 days. The products consisted largely of yellow-green plates of the title compound (75% yield), silvery polyhedra which proved to be tellurium metal, and clear polyhedra of TeO_2. Any attempts to make iron tellurites by reacting oxide-based iron compounds, such as FeO(OH) or Fe_3O_4, with TeO_2 resulted in mixtures of unidentified black polycrystalline powders.

Qualitative SEM elemental analysis verified the presence of Fe, Te, Cl, and O and confirmed the absence of any elements heavier than F.

Crystallography

A suitable single crystal was mounted onto the end of a glass fiber using quick-drying epoxy and was studied on a Nicolet R3m/V four circle diffractometer equipped with graphite monochromated Mo$K\alpha$ ($\lambda = 0.71073$ Å) radiation. An ω–2θ scan was utilized for room temperature data collection. Three standard reflections measured after every

0022-4596/99 $30.00

97 reflections indicated that the crystal was stable. A two-theta limit of 55° for data collection was employed. The intensity data were corrected for both Lorentz and polarization effects. Further data is included in Table 1.

The centrosymmetric space group, $P\bar{1}$ was chosen on the basis of lattice parameters and statistical tests and the subsequent successful refinement. The positions of the tellurium, iron, and chlorine atoms were determined using direct methods in SHELXTL-Plus (5). The oxygen atoms were found during successive Fourier syntheses. The structure was refined on $|F|$ by full, matrix least-squares techniques in SHELXTL-Plus. After absorption effects were compensated for by the use of empirical ψ-scan data (6) and an extinction parameter was applied (7), all atomic parameters were refined anisotropically. At this point, the hydrogen atoms were located using a Fourier map and were refined using a fixed position, group thermal parameter. No higher symmetry was detected using MISSYM algorithm within the PLATON program suite (8, 9). Final atomic coordinates and isotropic thermal parameters are shown in Table 2. Relevant atomic distances and angles are shown in Table 3.

TABLE 1
X-Ray Crystallographic Data for $H_3Fe_2(TeO_3)_4Cl$

Color, habit	yellow-green plate
Crystal size, mm^3	$0.05 \times 0.19 \times 0.26$
Space group	$P\bar{1}$
a (Å)	5.103(2)
b (Å)	6.653(2)
c (Å)	9.012(3)
α (°)	73.40(2)
β (°)	78.03(2)
γ (°)	76.76(2)
V (Å^3)	282.1(2)
Z	1
Formula weight (g/mol)	852.6
D_{calc} (g/cm^3)	5.018
μ (cm^{-1})	130.05
F (000)	376
2θ range (°)	3.5–55.0
Scan type	$\omega/2\theta$
Total reflns.	1457
Ind. reflns.	1309
Ind. reflns. ($F_o > 4\sigma(F_o)$)	1230
Refined parameters	90
Transmission factors	0.327–1.000
Extinction parameter	0.0015(3)
R^a, wR^b ($F_o > 4\sigma(F_o)$)	0.039, 0.050
R^a, wR^b (all data)	0.041, 0.051
S^c ($F_o > 4\sigma(F_o)$)	1.89
Max/min diff. peak (e/Å^3)	3.40/ − 2.47
Max/mean shift	0.001/0.000

[a] $R = \sum ||F_o| - |F_c|| / \sum |F_o|$.
[b] $wR = [\sum w\{|F_o| - |F_c|\}^2 / \sum w|F_o|^2]^{1/2}$; w, $1/[\sigma^2\{|F_o|\} + 0.0005\{|F_o|^2\}]$.
[c] $S = [\sum w\{|F_o| - |F_c|\}^2 / \{N_o - N_v\}]^{1/2}$; w, $1/[\sigma^2\{|F_o|\} + 0.0005\{|F_o|^2\}]$, N_o, number of observations; N_v, number of variables.

TABLE 2
Atomic Coordinates and Equivalent Isotropic Thermal Parameters (Å^2) for $H_3Fe_2(TeO_3)_4Cl$

	X	Y	Z	U_{eq}[a]
Te(1)	0.11979(8)	0.34044(6)	0.68799(5)	0.0075(2)
Te(2)	0.33835(9)	0.16583(7)	0.16942(5)	0.0088(2)
Fe	0.2761(2)	− 0.1452(2)	0.5560(1)	0.0073(3)
Cl	0	0	0	0.0176(8)
O(1)	0.193(1)	0.5924(7)	0.5385(6)	0.009(2)
O(2)	0.363(1)	0.1371(8)	0.5837(7)	0.012(2)
O(3)	0.405(1)	0.3164(8)	0.8056(6)	0.013(2)
O(4)	0.543(1)	0.2857(8)	0.2610(7)	0.013(2)
O(5)	0.113(1)	0.0379(8)	0.3552(6)	0.010(2)
O(6)	0.098(1)	0.4271(8)	0.1267(7)	0.015(2)
H(1)	0.4434	0.4443	0.8080	0.09(5)[b]
H(2)	0	$\frac{1}{2}$	0	0.09[b]

[a] $U_{eq} = \sum_i \sum_j (U_{ij} a_i^* a_j^* a_i \cdot a_j)$.
[b] Hydrogen atoms were refined isotropically as a group parameter.

Powder diffraction data (2θ = 5–70°) was obtained using a Scintag XDS 2000 θ/θ diffractometer equipped with monochromated Cu$K\alpha$ radiation (λ = 1.54056 Å). The powder pattern obtained was compared with a calculated pattern from the single crystal data, a pattern from an original study of rodalquilarite, and a pattern of the material reported as triclinic $Fe_2Te_4O_{11}$ (4). Lattice parameters were obtained from a least squares fit of 28 reflections (2θ = 10.40–65.66°).

Physical Characterization

The room temperature diffuse reflectance spectrum for $H_3Fe_2(TeO_3)_4Cl$ was measured from 2500 to 200 nm using a Shimadzu UV3100 spectrophotometer equipped with an integrating sphere attachment. Barium sulfate was used as the reflectance standard. The reflectance data were converted to absorbance data using the Kubelka–Monk function (10). The magnetic susceptibility data were collected using a Quantum Design SQUID magnetometer. Ground single crystals (30.2 mg) were placed in a gelatin pill capsule that was then held in a standard plastic drinking straw. Data were collected in a 0.1 T field from 5 to 300 K. The sample holder showed negligible diamagnetic effects on the bulk sample.

RESULTS AND DISCUSSION

We have prepared high quality crystals of the rare mineral rodalquilarite, $H_3Fe_2(TeO_3)_4Cl$, in good yield from $FeCl_2 \cdot 2H_2O$ and TeO_2 in a hydrothermal NH_4Cl solution. Ther procedure was similar to that used to attempt to prepare the iron analog of the spiroffite series $M_2Te_3O_8$. Other iron sources were investigated, as well as other

TABLE 3
Relevant Interatomic Distances (Å) and Angles (°) with ESD's for $H_3Fe_2(TeO_3)_4Cl$

Te(1)–O(1)		1.885(4)
–O(2)		1.930(5)
–O(3)		1.924(6)
–O(1)		2.725(6)
–O(6)		2.517(6)
–Cl	2×	3.113(1)
Te(2)–O(4)		1.876(7)
–O(5)		1.920(5)
–O(6)		1.872(5)
–O(2)		2.963(5)
–Cl	2×	3.075(1)
Fe–O(1)		1.943(6)
–O(2)		2.008(5)
–O(2)		2.115(6)
–O(4)		1.950(6)
–O(5)		2.028(5)
–O(5)		2.086(5)
H(1)–O(3)		0.924(6)
H(2)–O(6)	2×	1.267(6)

O(1)–Te(1)–O(2)	98.3(2)	O(2)–Fe–O(5)	157.9(2)
O(1)–Te(1)–O(3)	95.7(2)	O(2)–Fe–O(5)	84.9(2)
O(2)–Te(1)–O(3)	87.7(2)	O(2)–Fe–O(4)	84.7(2)
		O(2)–Fe–O(5)	85.6(2)
O(4)–Te(2)–O(5)	98.9(3)	O(2)–Fe–O(5)	88.1(2)
O(4)–Te(2)–O(6)	89.7(3)	O(4)–Fe–O(5)	104.9(2)
O(5)–Te(2)–O(6)	95.5(2)	O(4)–Fe–O(5)	172.1(2)
		O(5)–Fe–O(5)	77.7(2)
O(1)–Fe–O(2)	101.0(2)		
O(1)–Fe–O(2)	178.0(2)	O(6)–H(2)–O(6)	180.0(2)
O(1)–Fe–O(4)	93.8(2)		
O(1)–Fe–O(5)	93.6(2)	Te(1)–O(3)–H(1)	115.2(4)
O(1)–Fe–O(5)	93.4(2)		
O(2)–Fe–O(2)	80.4(2)	Te(2)–O(6)–H(2)	122.4(4)
O(2)–Fe–O(4)	90.8(2)		

mineralization conditions, and the only product was either the title compound in lesser yield or uncharacterizable black powders. No evidence of the iron analog of spiroffite was ever observed in our hands.

The high quality of the crystals enabled us to obtain a better data set and structure solution than that observed previously (2). This improved data quality enabled us to locate the hydrogen atoms in the structural refinement.

Structure

Rodalquilarite has a layered structure, shown in Fig. 1, with Fe–Te–O layers interconnected to one another through long Te–Cl contacts and O–H–O interactions. The layers in this structure run parallel to the *ab* plane and consist of FeO_6 octahedra and two crystallographically distinct TeO_3 pyramids. The FeO_6 octahedra show only

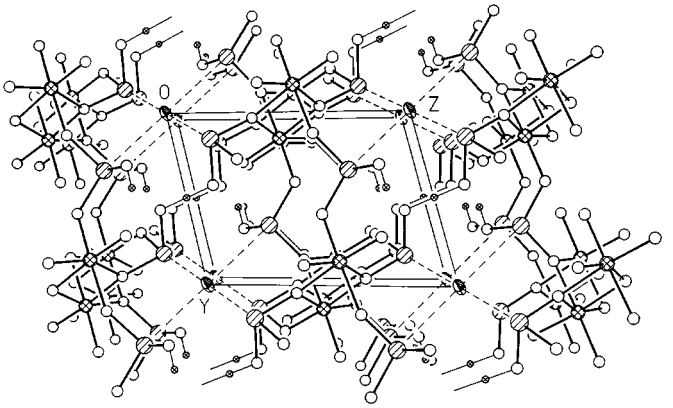

FIG. 1. Unit cell view of $H_3Fe_2(TeO_3)_4Cl$ shown down the *a* axis. The striped spheres are tellurium atoms, the large, cross-hatched spheres are iron atoms, the full thermal ellipsoids denote chlorine atoms, the open spheres are oxygen atoms, and the small cross-hatched spheres attached to neighboring atoms by thin bonds are hydrogen atoms.

modest distortions from ideality with Fe–O distances ranging from 1.943(6) to 2.086(5) Å, and O–Fe–O angles of 80.4(2)–104.9(2)° for adjacent oxygen atoms. These octahedra form zigzag chains in the *a* direction by edge-sharing with neighboring octahedra. Each of these chains are attached to the neighboring chains in the *b* direction by two equivalent TeO_3 pyramids. The TeO_3 pyramid is comparable to those in either $Ba_2Cu_4Te_4O_{11}Cl_4$ or $BaCu_2Te_2O_6Cl_2$ (11), with Te(1)–O distances of 1.885(4)–1.930(5) Å and O–Te(1)–O angles ranging from 87.7(2)° to 98.3(2)°. Two of the oxygen atoms (O(1) and O(2)) in this TeO_3 pyramid are shared between iron and tellurium atoms, whereas the third oxygen atom, O(3), has a terminal hydrogen atom (H(1)) attached with an H(1)–O(3) distance of 0.924(6) Å.

The second crystallographically distinct TeO_3 pyramid is primarily involved in connecting the layers together. As before, this TeO_3 pyramid is quite typical, with Te(2)–O distances ranging from 1.872(5) to 1.920(5) Å and O–Te(2)–O angles of 89.7(3)–98.9(3)°. As with the $Te(1)O_3$ pyramid, there are two oxygen atoms from this pyramid that are shared between iron and tellurium atoms, while there is a hydrogen atom attached to the third oxygen atom. Unlike before, this hydrogen atom is not terminal, but lies on an inversion center and connects TeO_3 pyramids across layers with H(2)–O(6) distances of 1.267(6) Å. This is an unusual arrangement, but often arises in hydrogen bonds with O–O distances less than appoximately 2.5 Å (12). Furthermore, it is predicted that the O–H–O geometry should be linear in situations where the O–O distance is less than 2.7 Å (13).

Additionally, the layers appear to also be held together by Te-Cl contacts. Although, each of these contacts is somewhat long (Te(1)–Cl = 3.113(1) Å, Te(2)–Cl = 3.075(1) Å), this nearly perfect square planar arrangement

(Te(1)–Cl– Te(2) angles = 87.6(1) or 92.4(1)°) appears to also provide structural stability. This longer interaction between tellurium and chlorine has been observed in other tellurium oxychlorides including $Te_6O_{11}Cl_2$ (14) and $Ba_3Te_2O_6Cl_2$ (15).

Bond Valence Sums

In an effort to confirm the proper assignment of hydrogen atoms, the correspondence between bond distance and bond valence (16) was used to determine the oxidation states of all atoms, excluding the weakly bound chlorine atom. By using the regular assignments of -1, -2, and $+1$ for chlorine, oxygen, and hydrogen, and by the assumption that tellurium in the TeO_3 or TeO_{3+1} unit is tetravalent, the oxidation state of the iron atom must be trivalent. The result of the calculations based on these assignments is shown in Table 4 and shows that there are no significant discrepancies in our proposed model.

Physical Properties

Diffuse reflectance spectroscopy was used to determine the optical band gap of our synthesized rodalquilarite. The plot of absorbance vs energy is shown in Fig. 2. The plot of (absorbance)^2 vs energy at the absorption edge (2.50–3.00 eV, correlation coefficient 0.994) has a better linear dependence than does the plot of (absorbance)$^{1/2}$ vs energy (correlation coefficient 0.916), which suggests that the material has a direct band gap (17). Therefore, the band gap was obtained extrapolating the plot of (absorbance)^2 vs energy to (absorbance)$^2 = 0$, which resulted in a band gap of 2.51 eV. There are also two very weak peaks corresponding to spin forbidden *d–d* transitions. The lower energy transition occurs at 1.42 eV (11.450 cm^{-1}) which can be tentatively assigned as the $^6A_{1g} \rightarrow {}^4T_{1g}$ transition, while the peak at 1.95 eV (15.720 cm^{-1}) probably arises due to the $^6A_{1g} \rightarrow {}^4T_{1g}$ transition (18). Additional transitions that have been previously observed in Fe^{3+} compounds occur at higher energies than the band transition in rodalquilarite and could not be seen in this study.

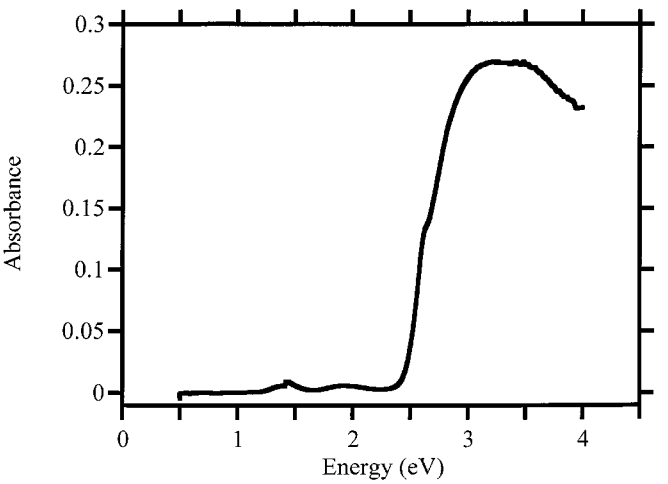

FIG. 2. Diffuse reflectance spectrum for $H_3Fe_2(TeO_3)_4Cl$, showing absorption edge and bands due to spin forbidden transitions at the transition metal center.

Magnetic susceptibility data were obtained on ground crystals of our synthetic rodalquilarite that were physically separated from their side products. This material displays Curie–Weiss behavior at higher temperatures and subsequently undergoes an antiferromagnetic transition with a Neel temperatures (T_N) of 29 K. By using a plot of χ^{-1} vs temperature (Fig. 3), the linear portion above T_N could be fit to Curie–Weiss behavior. The Curie–Weiss constants were $C = 10.21$ EMU-K/mol and $\theta = -97$ K. Using the Curie

TABLE 4
Valence Bond Sums for $H_3Fe_2(TeO_3)_4Cl$[a]

H(1)	0.89(1)
H(2)	0.707(8)
Fe(1)	2.99(2)
Te(1)	3.80(3)
Te(2)	3.81(3)
O(1)	1.89(2)
O(2)	2.03(2)
O(3)	2.05(2)
O(4)	1.91(3)
O(5)	2.06(2)
O(6)	1.91(2)

[a] $\sum s(M-L) = \sum \exp[(r_o - r)/0.37]$. s, individual bond valences; r, bond distance in structure; and r_o, empirically derived $M-L$ single-bond distance (Fe^{III}–O = 1.692, Te^{IV}–O = 1.759 Å). All distances from table found in Ref. (16).

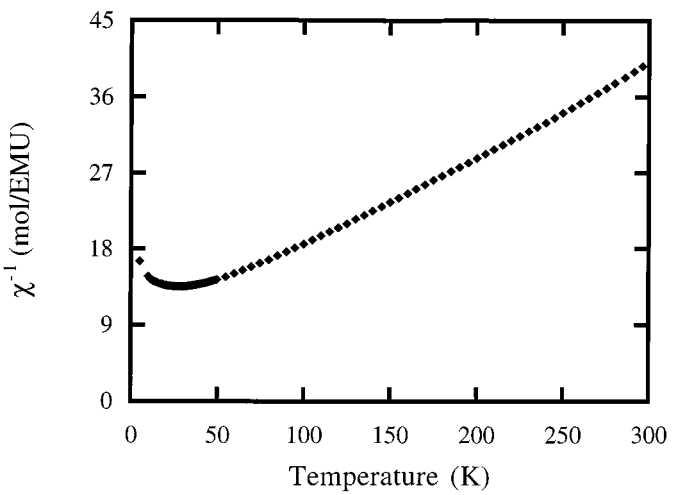

FIG. 3. Plot of the inverse magnetic susceptibility (χ^{-1}) vs temperature (K) for $H_3Fe_2(TeO_3)_4Cl$.

constant, a magnetic moment of 6.39 BM per Fe atom is obtained, which corresponds reasonably well with the spin-only calculated value of 5.92 BM/Fe^{3+} ion.

Powder Diffraction

The powder diffraction pattern of a bulk sample of the synthetic rodalquilarite was obtained as an additional check to confirm that the structural determination presented here is correct and that the bulk sample was phase pure. This pattern was indexed based on 28 reflections ($a = 5.108(5)$ Å, $b = 6.634(4)$ Å, $c = 8.987(4)$ Å, $\alpha = 73.52(4)^\circ$, $\beta = 78.10(5)$, $\gamma = 76.67(7)$, $V = 280.9$ Å^3) to approximately the same cell as was determined during the single crystal X-ray determination. In addition, Fig. 4 shows a comparison of our observed powder pattern with a pattern calculated from the single crystal structural data and the pattern obtained from a previously reported powder study of rodalquilarite (19) and they are all clearly identical. Also included in the figure is a powder pattern of a compound assigned as $Fe_2Te_4O_{11}$ without substantial further characterization (4). The fact that it is virtually superimposable upon the other three strongly suggests that these workers actually prepared rodalquilarite instead of a new form of $Fe_2Te_4O_{11}$.

CONCLUSION

We have prepared high quality crystals of the unusual mineral rodalquilarite in high yield via hydrothermal synthesis. A structural redetermination allowed us to locate the hydrogen bonds holding the layers together. In addition, we believe that the phase that was reported as triclinic $Fe_2Te_4O_{11}$ is actually rodalquilarite. We support this hypothesis with a comparison of the reported powder pattern

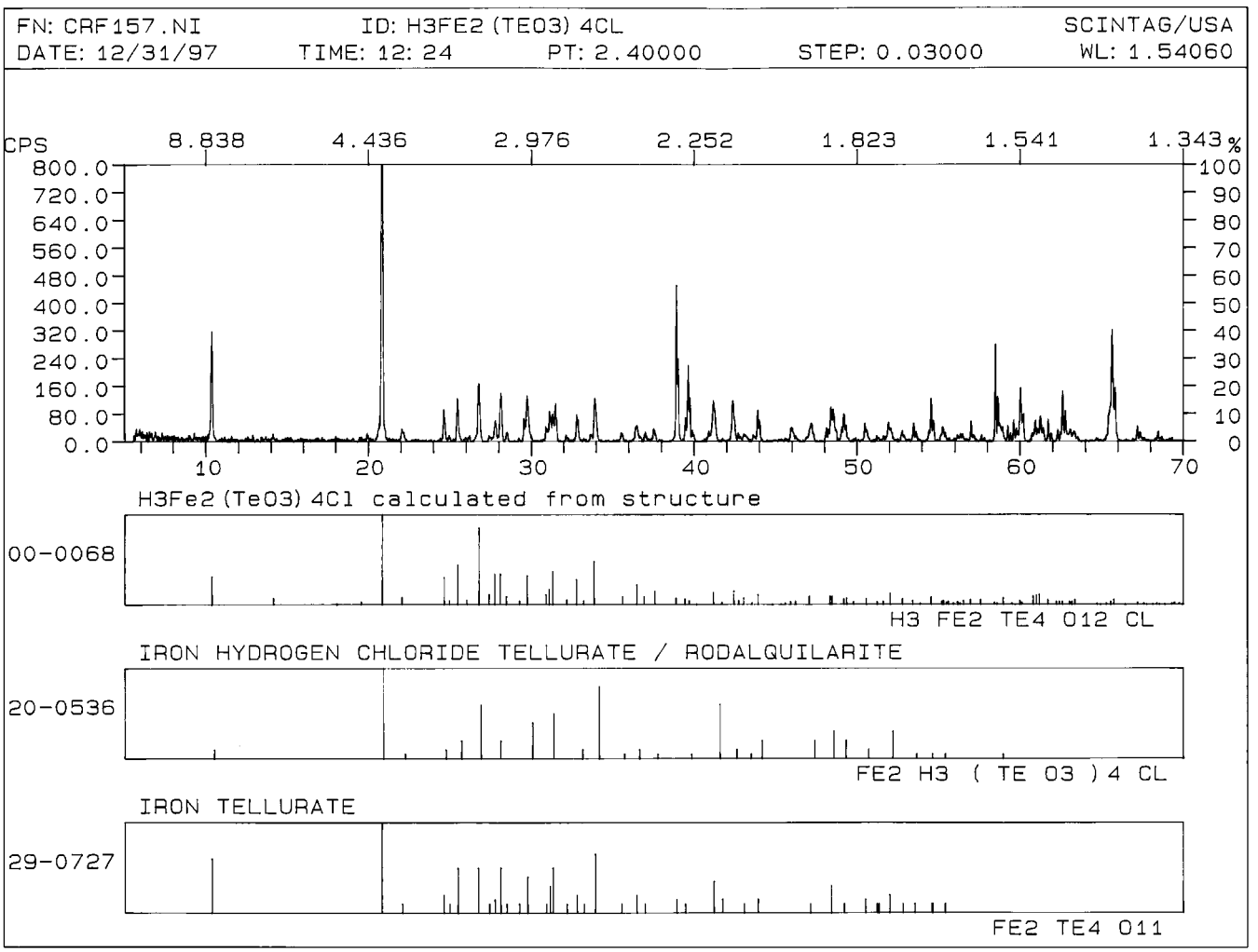

FIG. 4. X-ray powder diffraction pattern for $H_3Fe_2(TeO_3)_4Cl$. An experimental X-ray powder diffraction pattern is shown with cards of a calculated pattern from the single crystal X-ray results from this study on top, a previously reported powder diffraction pattern of rodalquilarite (17) in the middle, and a phase reported previously as $Fe_2Te_4O_{11}$ (4) on the bottom, which suggest that the phases in each study were rodalquilarite.

with both our single crystal X-ray data, as well as our X-ray powder diffraction pattern. No evidence of the iron analog of spiroffite, $M_2Te_3O_8$, has been observed. Attempts to synthesize this material using other iron starting materials such as Fe_3O_4, FeO(OH), or $Fe(NO_3)_3$ failed to yield the desired phase. In addition, attempts to alter composition through the varying of the nominal iron to tellurium ratio to date have failed to yield new iron tellurites.

ACKNOWLEDGMENTS

CRF thanks Dr. George L. Schimek for many valuable discussions. The work at Clemson University was supported by the National Science Foundation under Grant CHE-9102548, and the work at The Ohio State University was supported by the National Science Foundation under Grant DMR9357600 and by the U.S. Department of Energy, Midwest Superconductivity Consortium, under Contract DEFG02-90ER45427.

REFERENCES

1. C. R. Feger, G. L. Schimek, and J. W. Kolis, *J. Solid State Chem.* **143,** 246 (1999).
2. Y. Dusausoy and J. Protas, *Acta Crystallogr. B* **25,** 1551 (1969).
3. J. C. Jumas, L. Fournes, M. Wintenberger, and E. Philippot, *J. Solid State Chem.* **39,** 39 (1981).
4. R. Astier, E. Philippot, J. Moret, M. Maurin, *CR Acad. Sci. Paris, Ser. C* **280,** 1141 (1975).
5. G. M. Sheldrick, "SHELXTL-Plus," version 4.2 Structure Determination Software Program, Siemens Analytical X-ray Instruments, Inc., Madison, Wisconsin, 1990.
6. A. C. T. North, D. C. Phillips, and F. S. Mathews, *Acta Crystallogr. A* **24,** 351 (1968).
7. A. C. Larson, "Crystallographic Computing" (F. R. Ahmed, S. R. Hall, and C. P. Huber, eds), pp. 291–294. Munksgaard, Copenhagen, 1970.
8. Y. LePage, *J. Appl. Crystallogr.* **20,** 264 (1987).
9. A. L. Spek, *Acta Crystallogr. A* **46,** C34 (1990).
10. W. W. Wendlandt and H. G. Hecht, "Reflectance Spectroscopy." Interscience Publishers, New York, 1966.
11. C. R. Feger and J. W. Kolis, *Inorg. Chem.* **37,** 4046 (1998).
12. H. Effenberger, *J. Solid State Chem.* **233,** 107 (1996).
13. I. D. Brown, *Acta Crystallogr. A* **32,** 24 (1976).
14. W. Abriel, *Z. Naturforsch. B* **36,** 405 (1981).
15. D. Hottentot, B. O. Loopstra, *Acta Crystallogr. C* **39,** 1600 (1983).
16. I. D. Brown and D. Altermatt, *Acta Crystallogr. B* **41,** 244 (1985).
17. J. I. Pankove, "Optical Processes in Semiconductors." Prentice Hall, Inc., Englewood Cliffs, NJ, 1971.
18. C. J. Ballhausen, "Introduction to Ligand Field Theory." McGraw Hill, NewYork, 1962.
19. J. Sierra Lopez, G. Leal, R. Pierrot, Y. Laurent, J. Protas, and Y. Dusausoy, *Bull. Soc. Franc. Mineral. Cristallogr.* **91,** 28 (1968).